

Development of a Fingertip-sized Miniature X-ray Source Using a Laser-heated Pyroelectric Crystal

Satoshi Abo,^{a, †} Takahiro Uezato,^a Michiaki Takahashi,^b Fujio Wakaya^a

^a Graduate School of Engineering Science, Osaka University, 1-3 Machikaneyama, Toyonaka, Osaka 560-8531, Japan

^b School of Engineering Science, Osaka University, 1-3 Machikaneyama, Toyonaka, Osaka 560-8531, Japan

[†] Corresponding author: abo.satoshi.es@osaka-u.ac.jp

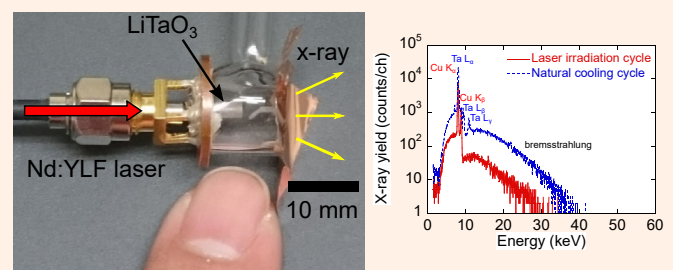
Received: 16 January, 2024; Accepted: 16 May, 2024; J-STAGE Advance Publication: 4 July, 2024; Published: 4 July, 2024

A pyroelectric crystal has spontaneous polarization and generates a high voltage of several tens of kilovolts between both ends of the crystal with a temperature change of several tens of degrees Celsius. When this pyroelectric crystal is set in a vacuum with a counter electrode, electrons can be accelerated by this high voltage. Such a device can be used as an X-ray source without any external high-voltage sources. In this study, a thin copper foil was set at the end of a vacuum chamber as a target electrode and partitioned between the vacuum and atmosphere. The pyroelectric crystal was heated using infrared (IR) laser light. The X-ray was detected outside the vacuum chamber. The X-ray yield and the maximum energy during the laser irradiation cycle were higher than those during the natural cooling cycle. A transmission X-ray image of the lead foil sandwiched between aluminum foils was observed outside the vacuum chamber. In addition, a fingertip-sized miniature X-ray source using the IR laser light through an optical fiber was used to heat the pyroelectric crystal. The sizes of the fingertip-sized miniature X-ray source were 10 mm in outer diameter and 10 mm in length. The X-ray yield and the maximum energy during the laser irradiation cycle were less than those during the natural cooling cycle, which differed from the experimental results obtained using the vacuum chamber. This was due to fewer electrons in the fingertip-sized miniature X-ray source and insufficient recovery of the compensating charge on the crystal surface during the natural cooling cycle.

Keywords Fingertip-sized miniature X-ray source; Pyroelectric crystal; Pyroelectric effect; Infrared laser

I. INTRODUCTION

A pyroelectric crystal exhibits spontaneous polarization, and its intensity is varied by the crystal temperature [1]. The spontaneous polarization on the crystal surface is canceled by a compensating charge from atmospheric air. Therefore, the electric potential on the crystal surface is zero and remains unchanged in the atmosphere. When the crystal is set in a vacuum with a counter electrode, the surface compensating charge excess and shortage due to temperature increase and decrease, respectively, resulting in voltage generation between the crystal surface and the counter electrode. The voltage depends on the pyroelectric coefficient, temperature change, and crystal size. Therefore, when the pyroelectric crystal has a high pyroelectric coefficient, the generated voltage reaches some tens of kilovolts with a temperature



change of several tens of degrees Celsius and a crystal size of several cubic-millimeters. The electrons on the crystal surface are desorbed and accelerated to the counter electrode by the generated high voltage. The accelerated electrons collide with the counter electrode and generate X-rays. This type of X-ray source was first developed by Brownridge [2, 3], where the temperature of the crystal was controlled using a resistive heating wire with current, a vacuum cryostat with a liquid nitrogen reservoir [2], and a Peltier device [3]. An X-ray source using a pyroelectric crystal initially has two major problems. One is the difficulty of realizing continuous X-ray emission because electron desorption and acceleration occur in conjunction with crystal heating and cooling cycles. This problem was pseudo cleared using a conical counter electrode and six pyroelectric crystals [4–6]. Another is that the size of the heating and cooling mechanism makes miniatur-

ization difficult. Because of the size of the crystal heating and cooling mechanism, the X-ray source miniaturization down to a few centimeters has been the limit so far [6]. Previously [6], the crystal was heated using a small heater and naturally cooled. Therefore, further miniaturization was not possible without changing the heating mechanism. To solve this problem, in our group, laser light is used to heat the pyroelectric crystal instead of the resistive heater or the Peltier device to downsize the X-ray source with the pyroelectric crystal [7, 8]. By miniaturizing the pyroelectric X-ray source to the size of a fingertip, it can be attached to the tip of an endoscope and can achieve X-ray irradiation inside the human body.

In our previous studies, the electron current from the crystal surface to the counter electrode by heating the pyroelectric crystal using pulsed ultraviolet laser light was measured [7], and the X-ray generation by continuous wave infrared (IR) laser light and its electron spot size on the counter electrode depended on the distance between the crystal surface and the counter electrode were discussed [8]. In this study, the energy spectrum and time dependence of X-ray extracted from the end of the vacuum chamber, X-ray transmission imaging outside the vacuum chamber, and fabrication and demonstration of a fingertip-sized miniature X-ray source with a size of approximately tens of cubic-millimeters and fiber-guided IR laser are discussed.

II. EXPERIMENTAL

Figure 1 shows the experimental setup used to measure the intensity and energy of the X-rays outside the vacuum chamber. A copper foil with a thickness of $10\ \mu\text{m}$ was set at the end of the vacuum chamber as the target electrode and partition between the vacuum and atmosphere. An X-ray detector [Amptek XR-100T-CdTe ($3 \times 3 \times 1\ \text{mm}^3$)] was positioned 10 mm away from the copper foil. The $-Z$ surface of a LiTaO₃ crystal was fixed on a copper plate with a center hole for laser irradiation. The $+Z$ surface of the crystal was 6 mm away from the copper foil because the maximum X-ray yield was obtained with a small-diameter target electrode in the previous study [8]. The diameter and thickness of the crystal were 5 and 4 mm, respectively. The crystal was heated by

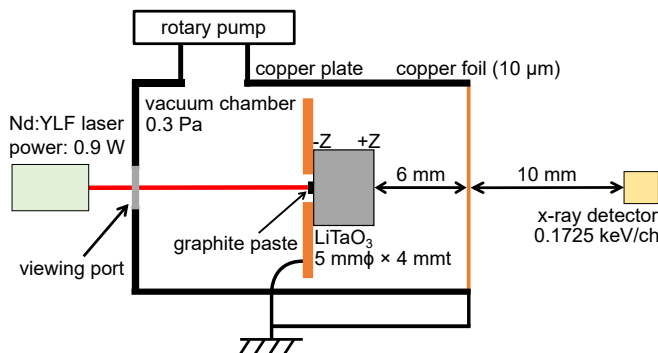


Figure 1: Experimental setup used to measure the intensity and energy of X-rays outside the vacuum chamber.

neodymium-doped yttrium lithium fluoride (Nd:YLF) laser light with a wavelength of 1047 nm and a power of 0.9 W. The LiTaO₃ crystal does not absorb laser light with a wavelength of 1047 nm [9]. Therefore, a thin carbon paste was coated as the light absorption layer at the center of the crystal. The pressure in the vacuum chamber was approximately 0.3 Pa because the maximum X-ray yield was expected at a pressure of the order of 10^{-1} Pa [10].

Figure 2 shows an optical image and a schematic of an object for X-ray transmission imaging. A cross-shaped lead foil was sandwiched between the aluminum foils. The thicknesses of the lead and aluminum foil were 0.3 and 0.1 mm, respectively. The X-ray mass attenuation coefficients of lead and aluminum for 10-keV X-ray were 1.306×10^2 , and $2.623 \times 10^1\ \text{cm}^2\ \text{g}^{-1}$, and 1.436×10^1 and $5.685 \times 10^{-1}\ \text{cm}^2\ \text{g}^{-1}$ for 40-keV X-ray, respectively [11–13]. From these values, the attenuation rates for the lead and aluminum foil were approximately 100% for the X-ray energies less than 40 keV and 50% for the X-ray energy of 10 keV, respectively. The X-ray transmission image was taken using an X-ray film (Fujifilm IXFR) attached to the object positioned 5 mm away from the copper foil. In the X-ray transmission imaging, 90-s laser irradiation and 90-s natural cooling cycles were repeated eight times.

Figure 3 shows a schematic of the fingertip-sized miniature X-ray source using LiTaO₃ crystal heated by a Nd:YLF

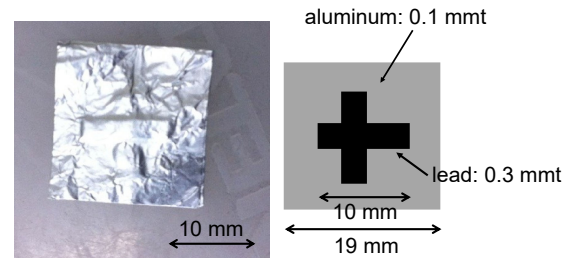


Figure 2: Optical image and schematic of the object for X-ray transmission imaging. Cross-shaped lead foil was sandwiched between the aluminum foils. The attenuation factors of 0.1-mm-thick aluminum and 0.3-mm-thick lead are approximately 50% for 10-keV X-ray and approximately 100% for <40-keV X-ray, respectively.

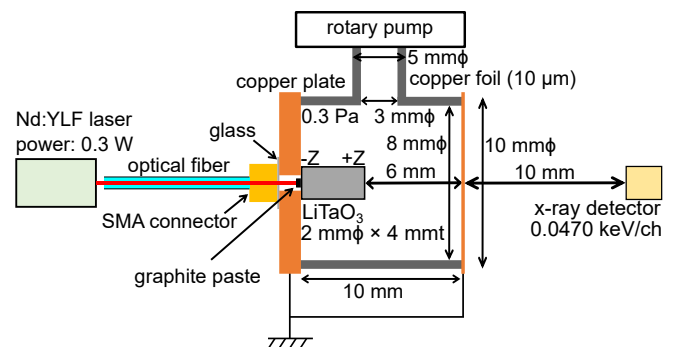


Figure 3: Schematic of the fingertip-sized miniature X-ray source using LiTaO₃ crystal heated using Nd:YLF laser light.

laser light. The outer part of the fingertip-sized miniature X-ray source was a borosilicate glass tube with inner and outer diameters of 8 and 10 mm, respectively. The length of the outer part was 10 mm. Both ends of the outer part were sealed with a copper foil with a thickness of 10 μm and a copper plate with a thickness of 1 mm. The copper plate had a 1-mm hole for passing through laser light and was sealed with a glass plate. The SMA connector was used to connect the optical fiber. The LiTaO_3 crystal with a thickness of 4 mm and a diameter of 2 mm was set at the center of the copper plate, resulting in the distance from the +Z surface of the crystal and the copper foil of 6 mm. Graphite paste was coated at the center of the -Z surface of the LiTaO_3 crystal as an absorption layer of the laser light, as in the experiment with the vacuum chamber. A glass tube with inner and outer diameters of 3 and 5 mm was connected to the side of the outer part of the X-ray source for evacuating air at a pressure of 0.3 Pa by a rotary pump. The X-ray detector [Amptek XR-100CR (13 mm²/500 μm , 1 mil Be window)] was placed 10 mm away from the copper foil. The power of the Nd:YLF laser light was 0.3 W, which was lower than that in the experiment with the vacuum chamber, to prevent crystal destruction due to thermal expansion.

III. RESULTS AND DISCUSSION

Figure 4 shows the time dependence of the X-ray yield outside the vacuum chamber for repeat 90-s laser irradiation and 90-s natural cooling cycles. The X-ray generated was synchronized with the laser irradiation and the natural cooling cycles. The X-ray yields at the laser irradiation cycles were higher than those at the natural cooling cycles. The energy spectra were also measured at the same time to verify where X-rays were generated.

Figure 5 shows the X-ray energy spectra for the first 90-s laser irradiation and the first 90-s natural cooling cycles in Figure 4. The total X-ray yield for the laser irradiation cycle was higher than that for the natural cooling cycle. The maximum X-ray energies for the laser irradiation and natural cooling cycles were 68 and 35 keV, respectively. This means that maximum voltages of 68 and 35 kV were generated between the crystal surface and the copper foil during the

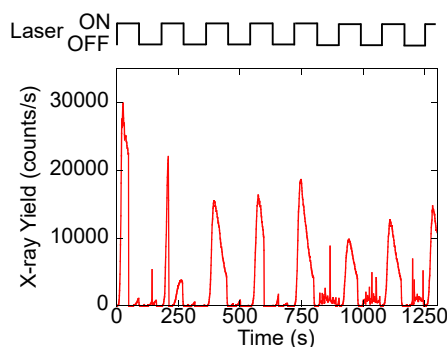


Figure 4: Time dependence of the X-ray yield for repeat 90-s laser irradiation and 90-s natural cooling cycles. The X-rays were mainly observed during the laser irradiation cycle.

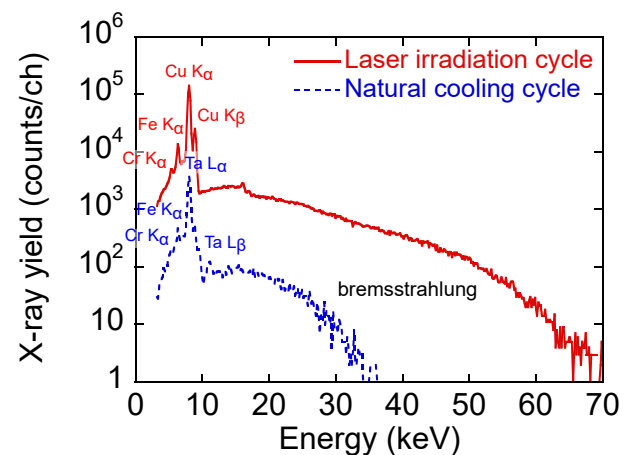


Figure 5: X-ray energy spectra for the first 90-s laser irradiation and the first 90-s natural cooling cycle in Figure 4. The characteristic X-rays for copper, iron, and chromium were detected during the laser irradiation cycle. The characteristic X-rays for tantalum, iron, and chromium were detected during the natural cooling cycle.

laser irradiation and natural cooling cycles. The characteristic X-rays for copper K α (8.048 and 8.028 keV), K β (8.905 and 8.977 keV), iron K α (6.404 and 6.391 keV), and chromium K α (5.415 and 5.405 keV) were detected during the laser irradiation cycle. The energies of the characteristic X-rays were taken from the tables by Firestone *et al.* [14, 15]. These results indicated that the electrons were desorbed from the crystal surface, accelerated, and collided with the copper foil. The characteristic X-rays for iron and chromium were presumably from the stainless-steel vacuum chamber by X-ray-induced X-ray emission. In contrast, the characteristic X-rays for tantalum L α (8.146 and 8.088 keV), L β (9.646, 9.875, and 9.316 keV), iron K α , and chromium K α were detected during the natural cooling cycle. These results indicated that the electrons were accelerated in the opposite direction during the laser irradiation cycle and collided with the surface of the LiTaO_3 crystal. The absorbed doses to water for laser irradiation and natural cooling cycles were 10.8 and 0.347 μGy , respectively, which were calculated with the detector size, detector sensitivity, and mass attenuation coefficient [16–18]. Because sufficient X-ray energy to expose the X-ray film was observed outside the vacuum chamber, the X-ray transmission image was taken by the pyroelectric X-ray source.

Figure 6 shows the X-ray transmission images using the X-ray film with and without the cross-shaped lead foil for eight repetition of 90-s laser irradiation and 90-s natural cooling cycles. The cross-shaped lead foil is clearly observed in Figure 6(a). In addition, half-transparent aluminum foil was also seen in both panels of Figure 6(a, b). This means that the X-ray source with a pyroelectric crystal is sufficiently usable for transmission imaging.

Figure 7 shows an optical image of the fingertip-sized miniature X-ray source. A glass tube with outer and inner diameters of 10 and 8 mm was used as the outer part of the X-ray source. The size of the fingertip-sized miniature X-ray

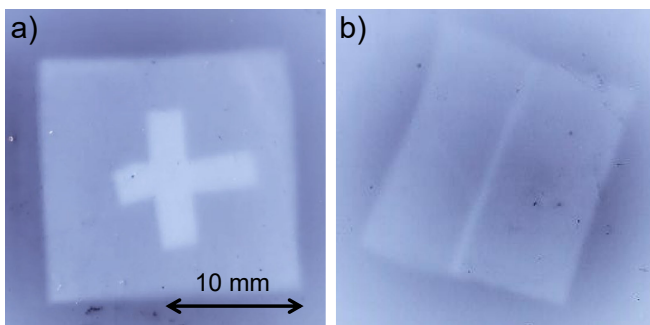


Figure 6: X-ray transmission images using the X-ray film (a) with and (b) without cross-shaped lead foils. The cross-shaped lead foil sandwiched with aluminum foil was clearly observed.

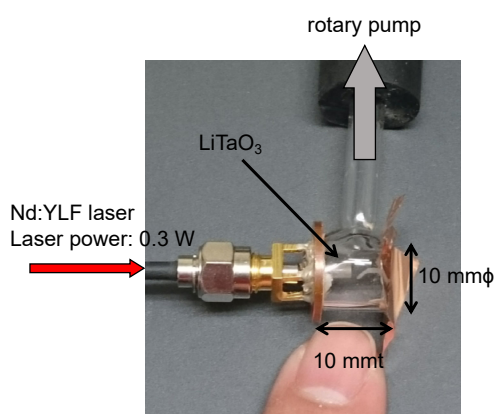


Figure 7: Optical image of the fingertip-sized miniature X-ray source.

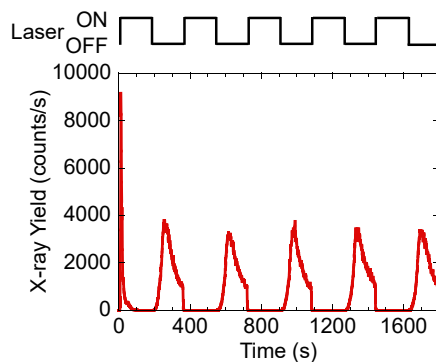


Figure 8: Time dependence of the X-ray yield from the fingertip-sized miniature X-ray source for repeated 180-s laser irradiation and 180-s natural cooling cycles. The X-rays were mainly observed during natural cooling cycles.

source was 10 mm in outer diameter and 10 mm in length. The copper plate and foil of the back and front sides were bonded using conductive glue. A rotary pump was used to create a vacuum in the X-ray source.

Figure 8 shows the time dependence of the X-ray yield from the fingertip-sized miniature X-ray source for repeated 180-s laser irradiation and 180-s natural cooling cycles. In the first laser irradiation cycle, a high X-ray yield was observed. However, from the second laser irradiation cycle,

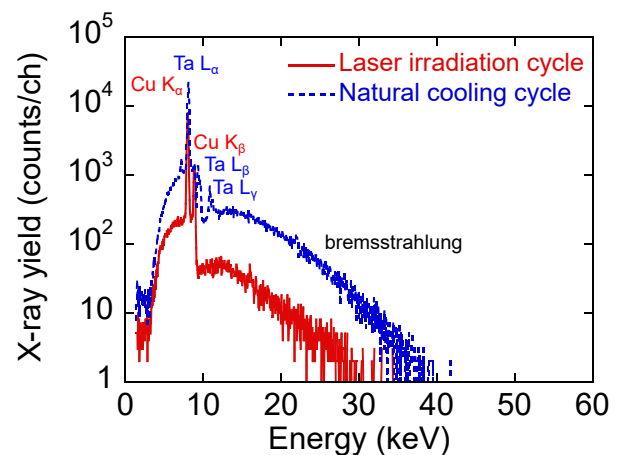


Figure 9: X-ray energy spectra from the fingertip-sized miniature X-ray source for the first 180-s laser irradiation and the first 180-s natural cooling cycles. Copper and tantalum characteristic X-rays were observed during laser irradiation and natural cooling cycles, respectively.

X-rays were rarely observed. In the natural cooling cycle, almost the same X-ray yields at every cycles were observed. In the experiment with a vacuum chamber (Figures 4 and 5), X-rays were mainly observed in the laser irradiation cycles. In contrast, in the experiment with the fingertip-sized miniature X-ray source, X-rays were mainly observed in the natural cooling cycles. This was presumably due to fewer electrons in the miniature X-ray source and insufficient recovery of the compensation charge on the crystal surface during the natural cooling cycle. In addition, since the housing of the miniature X-ray source is a glass tube, the charging of the glass tube and the difference in the distribution of the electric field from that with the vacuum chamber may also affect the X-ray generation.

Figure 9 shows the X-ray energy spectra from the fingertip-sized miniature X-ray source for the first 180-s laser irradiation and the first 180-s natural cooling cycles. In the laser irradiation cycle, only the characteristic X-rays for copper were observed because, unlike the experiment with the vacuum chamber, there was no stainless steel around the pyroelectric crystal. In the natural cooling cycle, only the characteristic X-rays for tantalum were observed, as in the laser irradiation cycle. This also indicated that the iron and chromium detected in the experiment with the vacuum chamber (Figure 5) were derived from the stainless steel used as the chamber material. The maximum X-ray energy for the laser irradiation cycle was lower than that for the natural cooling cycle. The absorbed doses to water for laser irradiation and natural cooling cycles were 0.742 and 2.74 μGy , respectively, which were calculated using the same method for the experiments with the vacuum chamber. The X-ray yield and the maximum energy from the fingertip-sized miniature X-ray source lower than those in the experiment with the vacuum chamber (Figures 4 and 5) were due to the smaller pyroelectric crystal and lower laser power. Therefore, it should be possible to increase the X-ray yield and energy

by using a larger pyroelectric crystal and heating it with a higher-power laser. As described above, a fingertip-sized miniature X-ray source using a pyroelectric crystal heated by IR laser light through an optical fiber was demonstrated.

IV. CONCLUSION

The X-ray yield and energy from the X-ray source using a LiTaO₃ crystal heated by IR laser light were measured outside the vacuum chamber. Higher X-ray yields and the maximum energy were observed during the laser irradiation cycle than those during the natural cooling cycle. The X-ray transmission image of the lead foil sandwiched between aluminum foils was taken outside the vacuum chamber with the X-ray source using a LiTaO₃ crystal heated by the IR laser light. In addition, a fingertip-sized miniature X-ray source was fabricated, and its characteristic was measured. A higher X-ray yield and the maximum energy were observed during the natural cooling cycle than those during the laser irradiation cycle, which differed from those with the vacuum chamber. This X-ray source can be attached to the tip of an endoscope to irradiate X-rays inside the human body.

Acknowledgments

This study was partly supported by JSPS KAKENHI Grant Number 23360022 and the Asahi Glass Foundation.

Note

This paper was presented at the 14th International Vacuum Electron Sources Conference (IVESC 2023) (University of Tsukuba, Tsukuba, Japan, September 25–29, 2023).

References

- [1] S. B. Lang, *Sourcebook of Pyroelectricity* (Gordon and Breach Science Publishers, New York, 1974) Chapter I Fundamentals of Pyroelectricity.
- [2] J. D. Brownridge, *Nature* **358**, 287 (1992).
- [3] J. D. Brownridge and S. Raboy, *J. Appl. Phys.* **86**, 640 (1999).
- [4] H. Mizota, Y. Nakanishi, H. Oohashi, Y. Ito, T. Tochio, S. Yoshikado, and T. Tanaka, *Radiat. Phys. Chem.* **75**, 1626 (2006).
- [5] H. Honda, S. Fukao, Y. Guan, Y. Nakanishi, Y. Sato, Y. Ito, and S. Yoshikado, *IOP Conf. Ser.: Mater. Sci. Eng.* **18**, 092034 (2011).
- [6] S. Yoshikado, *Isotope News* **737**, 12 (2015) (in Japanese).
- [7] T. Kisa, K. Murakami, S. Abo, F. Wakaya, M. Takai, and T. Ishida, *J. Vac. Sci. Technol. B* **28**, C2B27 (2010).
- [8] K. Nakahama, M. Takahashi, S. Abo, F. Wakaya, and M. Takai, *J. Vac. Sci. Technol. B* **32**, 02B108 (2014).
- [9] E. D. Palik (Ed.), *Handbook of Optical Constants of Solid III* (Academic Press, San Diego, 1998) p. 777.
- [10] J. D. Brownridge and S. M. Shafroth, *Appl. Phys. Lett.* **83**, 1477 (2003).
- [11] J. H. Hubbell, *Int. J. Appl. Radiat. Isot.* **33**, 1269 (1982).
- [12] J. H. Hubbell and S. M. Seltzer, *Tables of X-Ray Mass Attenuation Coefficients and Mass Energy-Absorption Coefficients 1 keV to 20 MeV for Elements Z = 1 to 92 and 48 Additional Substances of Dosimetric Interest*, NISTIR 5632 (National Institute of Standards and Technology, Gaithersburg, MD, 1995).
- [13] J. H. Hubbell and S. M. Seltzer, *X-Ray Mass Attenuation Coefficients: NIST Standard Reference Database 126*, Ver. 1.4 (National Institute of Standards and Technology, Gaithersburg, MD, 2004).
- [14] R. B. Firestone, V. S. Shirley, C. M. Baglin, S. Y. F. Chu, and J. Zipkin (Eds.), *Table of Isotopes Eighth Edition* (John Wiley & Sons Inc., New York, 1996) Appendix F, Table 7 x-ray energies and intensities.
- [15] E. Browne and R. B. Firestone, in: *Table of Radioactive Isotopes*, edited by V. S. Shirley (John Wiley & Sons Inc., New York, 1986) Appendix C, Table 7 x-ray energies and intensities.
- [16] C. T. Chantler, *J. Phys. Chem. Ref. Data* **24**, 71 (1995).
- [17] C. T. Chantler, *J. Phys. Chem. Ref. Data* **29**, 597 (2000).
- [18] C. T. Chantler, K. Olsen, R. A. Dragoset, J. Chang, A. R. Kishore, S. A. Kotochigova, and D. S. Zucker, *X-Ray Form Factor, Attenuation, and Scattering Tables: NIST Standard Reference Database 66*, Ver. 2.1 (National Institute of Standards and Technology, Gaithersburg, MD, 2005).



All articles published on e-J. Surf. Sci. Nanotechnol. are licensed under the Creative Commons Attribution 4.0 International (CC BY 4.0). You are free to copy and redistribute articles in any medium or format and also free to remix, transform, and build upon articles for any purpose (including a commercial use) as long as you give appropriate credit to the original source and provide a link to the Creative Commons (CC) license. If you modify the material, you must indicate changes in a proper way.

Copyright: ©2024 The author(s)

Published by The Japan Society of Vacuum and Surface Science